AFRL-PR-WP-TP-2006-259

CONTROL OF PENETRATION AND MIXING OF AN EXCITED SUPERSONIC JET INTO A SUPERSONIC CROSS STREAM (POSTPRINT)

S. Murugappan, E. Gutmark, and C. Carter

OCTOBER 2006

Approved for public release; distribution is unlimited.

STINFO COPY

PROPULSION DIRECTORATE
AIR FORCE MATERIEL COMMAND
AIR FORCE RESEARCH LABORATORY
WRIGHT-PATTERSON AIR FORCE BASE, OH 45433-7251

REPORT DOCUMENTATION PAGE

Form Approved
OMB No. 0704-0188

1. REPORT DATE *(DD-MM-YY)*	2. REPORT TYPE	3. DATES COVERED *(From - To)*
October 2006	Journal Article Postprint	N/A

4. TITLE AND SUBTITLE
CONTROL OF PENETRATION AND MIXING OF AN EXCITED SUPERSONIC JET INTO A SUPERSONIC CROSS STREAM (POSTPRINT)

5a. CONTRACT NUMBER
In-house

5b. GRANT NUMBER

5c. PROGRAM ELEMENT NUMBER
61102F

6. AUTHOR(S)
S. Murugappan and E. Gutmark (University of Cincinnati)
C. Carter (AFRL/PRAS)

5d. PROJECT NUMBER
2308

5e. TASK NUMBER
AI

5f. WORK UNIT NUMBER
00

7. PERFORMING ORGANIZATION NAME(S) AND ADDRESS(ES)

University of Cincinnati
Department of Aerospace Engineering
and Engineering Mechanics
Cincinnati, OH 45221-0070

Propulsion Sciences Branch (AFRL/PRAS)
Aerospace Propulsion Division
Propulsion Directorate
Air Force Research Laboratory
Air Force Materiel Command
Wright-Patterson AFB, OH 45433-7251

8. PERFORMING ORGANIZATION REPORT NUMBER
AFRL-PR-WP-TP-2006-259

9. SPONSORING/MONITORING AGENCY NAME(S) AND ADDRESS(ES)

Propulsion Directorate
Air Force Research Laboratory
Air Force Materiel Command
Wright-Patterson AFB, OH 45433-7251

10. SPONSORING/MONITORING AGENCY ACRONYM(S)
AFRL-PR-WP

11. SPONSORING/MONITORING AGENCY REPORT NUMBER(S)
AFRL-PR-WP-TP-2006-259

12. DISTRIBUTION/AVAILABILITY STATEMENT
Approved for public release; distribution is unlimited.

13. SUPPLEMENTARY NOTES
Journal article published in the Physics of Fluids, Vol. 17 (2005), published by the American Institute of Physics.

PAO case number: AFRL/WS 04-1384; Date cleared: 09 Dec 2004.

14. ABSTRACT
Rayleigh/Mie scattering from flow field ice crystals was used to study mixing and penetration of a forced a supersonic jet in a supersonic Mach-2 cross stream. Instantaneous images—using image planes along side-view and normal end-view to the flow axis—were used to study the dynamical structures in the jet whereas ensemble images provide information regarding the jet trajectory. Standard deviation images reveal information about the large-scale mixing/entrainment. Probability density functions were used to evaluate the mixing along the time-average jet interface. Forced cases indicate the presence of periodic formation of large-scale eddies in the jet/free stream interface. The eddies were bigger in size and more convoluted in the forced cases as compared to the baseline. These provided high penetration of the jet into the free stream. Forced cases also show higher region involved in small scale and/or bulk mixing in both the side- and end-views.

15. SUBJECT TERMS

16. SECURITY CLASSIFICATION OF:			17. LIMITATION OF ABSTRACT:	18. NUMBER OF PAGES	19a. NAME OF RESPONSIBLE PERSON (Monitor)
a. REPORT	b. ABSTRACT	c. THIS PAGE			Campbell D. Carter
Unclassified	Unclassified	Unclassified	SAR	20	19b. TELEPHONE NUMBER *(Include Area Code)* N/A

Standard Form 298 (Rev. 8-98)
Prescribed by ANSI Std. Z39-18

Control of penetration and mixing of an excited supersonic jet into a supersonic cross stream

S. Murugappan and E. Gutmark
Department of Aerospace Engineering and Engineering Mechanics, University of Cincinnati, Cincinnati, Ohio 45221-0070

C. Carter
AFRL/PRAS, 1950 Fifth Street, Wright-Patterson Air Force Base, Ohio 45433

(Received 11 April 2005; accepted 16 August 2005; published online 11 October 2005)

Rayleigh/Mie scattering (from flow-field ice crystals) was used to study mixing and penetration of a forced supersonic jet in a supersonic Mach (M)-2 cross stream. Instantaneous images—using image planes along (side-view) and normal (end-view) to the flow axis—were used to study the dynamical structures in the jet whereas ensemble images provide information regarding the jet trajectory. Standard deviation images reveal information about the large-scale mixing/entrainment. Probability density functions were used to evaluate the mixing along the time-average jet interface. Forced cases indicate the presence of periodic formation of large-scale eddies in the jet/free stream interface. The eddies were bigger in size and more convoluted in the forced cases as compared to the baseline. These provided high penetration of the jet into the free stream. Forced cases also show a larger region involved in small scale and/or bulk mixing in both the side—and end-views. Different metrics such as total area contained in the jet (A_{90}), total area involved in fluctuations of $\geqslant 30\%$ within the jet boundary ($A_{\sigma,30}$) and the interfacial contact at the jet free stream interface (S) were used to quantify the mixing of the forced cases. Analysis of averaged and standard deviation of end-view images indicates that these parameters were higher for the forced cases as compared to the baseline case. © *2005 American Institute of Physics*. [DOI: 10.1063/1.2099027]

I. INTRODUCTION

The scramjet propulsion concept requires rapid mixing between fuel and air, due to the limited time and space available for mixing and reaction in the combustor. A major difficulty is achieving simultaneous penetration of the fuel jet into the high-speed cross stream air and intense mixing between them to ensure efficient combustion. Additional performance factors such as combustion efficiency, reduction of emissions, improved flammability limits, and combustion stability are all governed by the completeness of the mixing process between fuel and air.

In the present study Rayleigh/Mie scattering visualizations were used to characterize the mixing characteristics of a high frequency actuator (HFA) in M-2 cold cross stream. The following section deals with the findings by other researchers on the transverse jet in cross flow using various flow visualization techniques, while subsequent sections discuss the different fuel injection strategies in scramjet combustors.

Planar laser-induced fluorescence (PLIF) or Rayleigh/Mie scattering has been used by several investigators to visualize the turbulent nature of transverse jet injection into supersonic cross flow.[1–4] Lee *et al.*[1] studied reacting and nonreacting transverse jets using OH-PLIF and NO-PLIF, respectively. OH images indicated that the combustion primarily took place in the shear layer formed by the jet and free stream, and in the boundary layer adjacent to the injection wall. Experiments in Refs. 2–4 were conducted in nonreacting flow conditions. Hermanson and Winter[2] used Mie scattering and spark schlieren photography to visualize a sonic jet in a M-2 cross stream. They observed structures that develop at the jet/free stream interface which persist far downstream in the instantaneous images. Gruber *et al.*[3] studied sonic transverse injection from circular and elliptic nozzles into a supersonic flow using Rayleigh/Mie scattering. They observed axis-switching phenomena with the elliptical nozzle that enhanced the lateral spread of the jet but reduced penetration by 20% when compared to the traditional circular injector. Vanlerberghe *et al.*[4] reported the mixing characteristics of an underexpanded jet in M-1.6 cross flow. A counter-rotating vortex pair observed in the jet plume was identified to play an important role in enhancing mixing in the wake region downstream of the barrel shock. They also reported that time-averaged images greatly overestimate the actual level of instantaneous mixing in the flow field. In all these studies[1–4] large-scale structures in the single-shot images were observed, which are not apparent in the frame-averaged images, thus emphasizing the need to understand the dynamic nature of the flow field. Although studies[1–4] were aimed primarily at understanding the flow dynamics of a transverse jet (elliptical and/or circular jet) in a cross stream, several investigators have identified other injection schemes that could be used to enhance mixing. The following sections present a brief overview of the traditional fuel injection schemes and other passive fuel strategies for scramjet applications.

There are two widely used fuel injection strategies in scramjet combustors: transverse and parallel injections.

Transverse injection may produce good penetration but is inevitably accompanied by shocks, which reduce the total pressure. Parallel injection on the other hand has lower total pressure losses and provides enhanced thrust but poor penetration into the cross stream.[5] Due to inherent drawbacks in the two traditional injection techniques, many researchers have suggested passive and active control techniques to enhance mixing at high speeds. A comprehensive review of different mixing enhancement techniques has been provided in Refs. 6 and 7 and is briefly summarized in the following.

Shock structures that are inherent in high-speed flow are a way of inducing vortex breakdown.[8] The interaction of the streamwise structures with the planar, oblique, or normal shock front causes vortex bursting due to the adverse pressure gradient imposed by the shock waves, generating high turbulence that enhances mixing. Menon[9] experimentally studied shock-wave induced mixing enhancement for scramjet combustors. Nitrogen was used to simulate the oxidizer while helium was used to simulate the fuel (hydrogen). The helium was injected parallel over a rearward facing step that acted as a flame holder. A small wedge was used to generate an oblique shock. Concentration measurements derived from planar Rayleigh scattering indicated a substantial increase in mixing with shock interaction.

Injectors that generate axial vorticity have been reported to enhance mixing. For example, a ramp fuel injector has been studied by Rogers *et al.*[10] Flow over a ramp produces vorticity due to the baroclinic torque, which enhances mixing and combustion efficiency. Marble *et al.*[11] used a lobed mixer for scramjet applications. Fuel is injected through the lobes at a small angle to the base wall. The air is ducted between the lobes and goes through an expansion wave as it is directed with a small angle to the base wall. Streamwise vorticity is generated along the entire periphery of the exhaust lip where fuel and air meet. This leads to high mixing efficiency, but suffers from aerodynamic pressure losses due to the squared geometry of the lobe. A good lobe geometry design requires no flow separation to induce vorticity and excellent aerodynamic performance.

Cutler and Doerner[12] studied the combined effect of swirl and injection angle of a supersonic low-molecular-weight gas (simulating hydrogen fuel) injected into a supersonic air stream. The mass fraction of the injectant obtained from a gas sampling probe in the cross stream was used to characterize mixing and penetration. A steady flow was assumed in their studies for evaluating the penetration depth and mixed mole fraction. They observed a minimal increase in mixing in the near field with a slight reduction in penetration. Both swirl and skew had little effect on mixing far downstream.

Forcing the jet in a cross stream has also been used to manipulate the jet shear layer characteristics. Recently Narayanan *et al.*[13] studied the effect of forcing of a subsonic jet in a subsonic cross stream. Velocity spectra from studies of an unforced flow were used as a tool to choose the excitation frequency they would use with the forced jet. Narayanan *et al.*[13] observed that the jet excited higher broadband frequencies in the near field. The far field was dominated by lower broadband spectra peaks. They showed that exciting a jet at higher frequencies could improve jet spread in the near field, whereas lower frequency enhanced the entrainment and mixing in the far field in an incompressible flow. Eroglu and Breidenthal[14] investigated pulsed jet in cross flows. Distinct vortex rings were observed when the flow rate of the jet was periodically modulated by a square wave. The strength and spacing of these vortex rings were found to be a function of the pulsing frequency for a given jet and cross flow combination. Their experiments indicate up to 70% increase in jet penetration and 50% reduction in flame length of the jet when compared to a steady jet. The effect of duty cycle and forcing frequency was studied by Hermanson *et al.*[15] and Johari *et al.*[16] The results suggest that the penetration of a fully modulated jet in cross flow could be characterized into two independent quantities. The injection time which corresponds to the period of excitation influences the jet structure at the injector with shorter times corresponding to compact vortex rings providing higher penetration and longer times to more diffuse turbulent puff-like structures. The duty cycle impacts the distance between the jet puffs or vortices near the injector, with higher values of duty cycle leading to more intense interaction between the turbulent jet puffs and correspondingly less jet penetration. In Refs. 13–16 flows were subsonic and forcing frequencies were <20 Hz, except with Ref. 13 where the highest forcing frequency was 1.5 kHz. All indicated an enhancement in penetration and mixing rate with forcing. Randolph *et al.*[17] investigated the effect of forcing of a transverse jet in a supersonic cross flow. The frequency of the forcing jet was chosen to be 1 Hz. They report a 12% increase in penetration when compared with a steady jet of the same peak exit pressure. The current study is an effort to evaluate the effect jet penetration and mixing of transversely injected high-frequency high-amplitude forced supersonic jet in a supersonic cross stream. The HFA was employed as an injector. It is capable of producing an SPL ≈ 135 dB [sound pressure level $=20\log(P_{\mathrm{rms}}/P_{\mathrm{ref}})$, where P_{rms}=RMS of pressure and P_{ref}=reference pressure, 20 μPa] and high-frequency (2–35 kHz) pressure and velocity oscillations. The details of its construction, design and flow-field characteristics can be found in Ref. 18.

II. EXPERIMENTAL SETUP

The experiments reported here were performed in the supersonic research facility at Wright Patterson Air Force Base. The details of the wind tunnel are provided in Ref. 19. A summary of the important features is presented in the following.

A continuous supply of pressurized air enters the inlet section of the tunnel and flows into the settling chamber. This section houses flow conditioning elements and sensors to measure stagnation pressure and temperature of the free stream. The air enters into the test section (cross section 0.131×0.152 m) through a two-dimensional nozzle section at a nominal Mach number of 2. The HFA was used as a fuel injector in the present study. The device is capable of producing high frequency, intense pulsation of the order of kilohertz (2–35 kHz). The device is compact, rugged, and simple and is suitable for high Reynolds number flow control

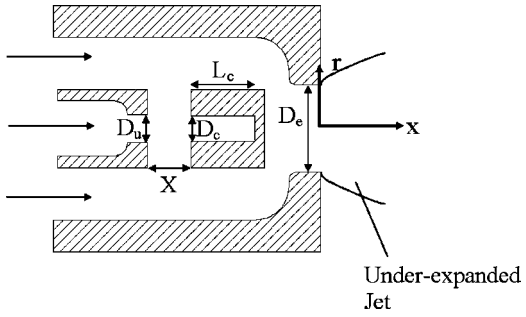

FIG. 1. Schematic of high frequency actuator.

applications. The schematic of the HFA is given in Fig. 1. The input to the actuator is a constant air mass flow rate at a certain pressure and temperature. The output is a circular jet with fluctuating flow in the axial direction superimposed on the mean field. The underexpanded air jet with the integrated HFA is shown in Fig. 1. A Hartmann-Sprenger (H–S) tube[20–23] is the internal excitation device upstream of the supersonic jet nozzle with an exit diameter, D_e, of 15.25 mm. The internal H–S excitation device was held together by struts inside the nozzle. The presence of struts caused an initial perturbation in the flow which decayed past 0.8 jet diameters. Different parameters of the H–S tube include D_u, jet diameter, D_c, cavity diameter, L_c, cavity length and X, standoff distance between the jet and the cavity. A parametric study of these parameters was conducted in Ref. 23 to optimize, D_u, D_c, and X. The H–S tube could be used to excite two different modes. The first mode referred to as jet regurgitant (JRG) mode involves periodic swallow and discharge of the jet at the cavity quarter wave mode frequency ($=C/4L_c$, where C is the speed of sound). The second mode is called the screech mode (not the same as screech observed in a supersonic jet), which is characterized by an oscillating shock standing in front of the cavity.[22] In the current study, D_u, D_c, and X were kept fixed, cavity length, L_c, was alone varied to excite different frequencies. The HFA was tuned to excite the JRG mode in the current experiments. Velocity and acoustic pressure power spectral density of the HFA excited at a nondimensional frequency of $\mathrm{St}_D=fD_e/U=0.09$ (where f is the frequency and U is the jet exit velocity) are shown in Fig. 2. The velocity spectra were measured on the center line at $x/D_e=2.5$. Both velocity and pressure spectra show a dominant peak at the excitation frequency.

A schematic of a transverse jet injected into a cross stream is shown in Fig. 3.[24] This figure indicates the streamwise (x) and transverse (y) coordinates; the spanwise (z) direction is perpendicular to the plane of the paper. Figure 3 also emphasizes the important flow features:

The jet interacts with the cross flow producing a three-dimensional bow shock before turning downstream;

A separation bubble is formed upstream of the jet due to the interaction of the bow shock with the free stream boundary layer;

Acceleration of the underexpanded jet into the cross flow introduces a barrel shock, which terminates at a Mach disk;

A second separation region develops downstream of the jet at the boundary layer reattachment point.

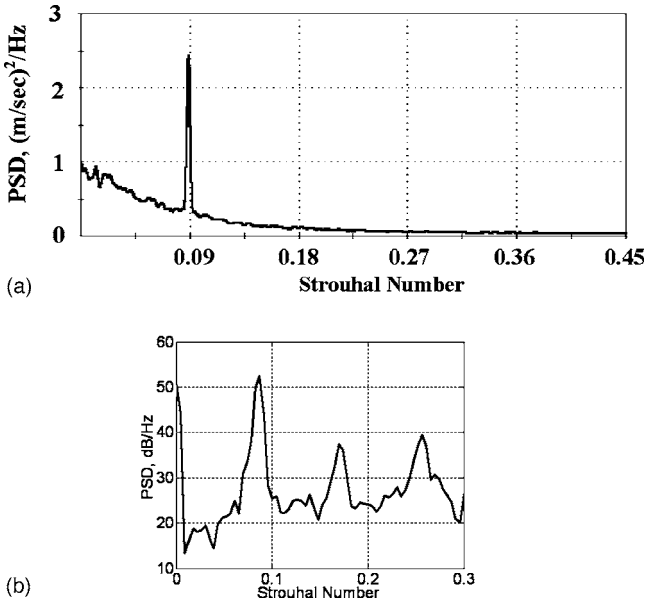

FIG. 2. (a) Axial velocity Power Spectral Density (PSD) at $M=1.57$, St $=0.09$, and $x/d_j=2.5$. (b) Acoustic pressure PSD at $M=1.57$, St$=0.09$, $x/D_j=16.7$, and 45 (upstream).

The penetration of the jet has been found to be a strong function of momentum flux ratio by Papamoschou and Hubbard.[25] The transverse jet eventually spreads and mixes with the free stream fluid as it is turned by the cross flow in the streamwise direction.

A. Laser diagnostics

Instantaneous measurements of the mixing regions were obtained using Mie scattering from the flow-field ice crystals. The ice crystals form naturally in the cold air from water vapor remaining in the flow stream (though the air is relatively dry). Strong scattering signals were recorded in the core flow from the small and abundant ice particles, while the pure injectant fluid had low scattering signal (only background scattering), as its source was dry compressed air. The laser-beam wavelength was 226 nm (to access NO A-X transitions for another experiment involving laser-induced fluorescence). The laser-beam energy was continuously monitored using a photodiode (displaying the signal on an oscilloscope).

The laser sheet was formed using a pair of lenses, a plano-concave cylindrical lens (−50 mm focal length) and a plano-convex spherical lens (1000 mm focal length). This

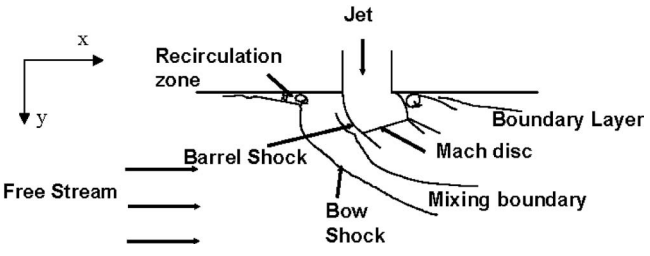

FIG. 3. Schematic of a transverse supersonic jet in a supersonic cross flow (Ref. 24).

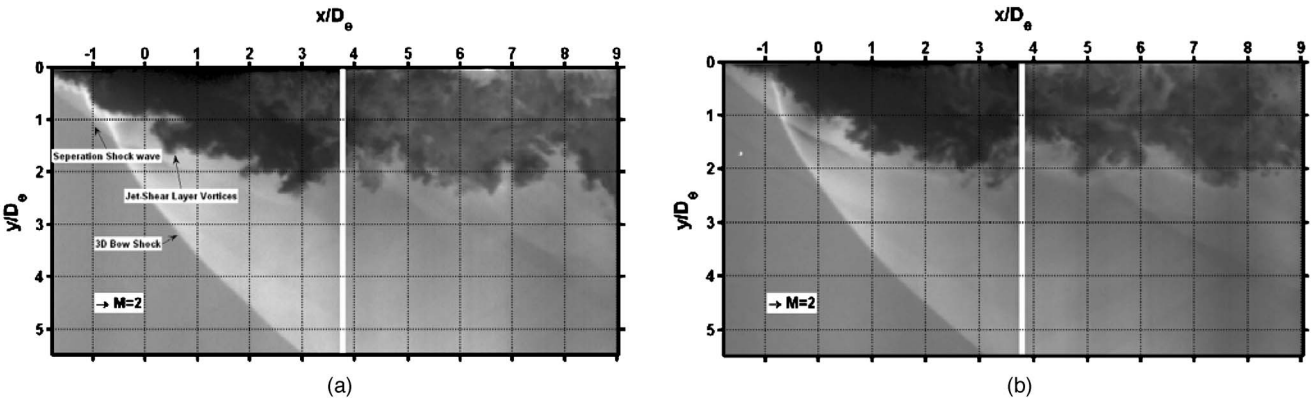

FIG. 4. Side-view images of instantaneous jet/free stream mixing: no forcing (baseline). The (a) left- and (b) right-hand images are uncorrelated, and the total field of view of $\sim 5.5 \times 9 D_e$ is composed of two probe locations (again making the two images independent).

arrangement resulted in a sheet height of about 75 mm. A Princeton Instruments PIMAX intensified CCD camera with a 512 by 512 pixel array was used to detect the scattering; to improve both signal strength and framing rate, the array pixels were binned 2 by 2 (before readout). The camera was fitted with a UV lens (a 45 mm focal length $f/1.8$ Cerco lens). For the end-view images, this sheet was directed across the span of the test section through fused silica windows, and the resulting fluorescence was imaged off-normal to the sheet using a schiempflug mount to mitigate image blur. For the side-view images, the laser sheet was directed through a fused-silica window forming the bottom floor of the wind tunnel, and the scattering was view in a normal-imaging configuration (schiempflug mount not needed). The laser sheet thickness was estimated to be 250–300 μm. The transmitting and receiving optical hardware were positioned on a traversing table allowing remote positioning of the measurement volume at any desired station in the flow field.

B. Operating conditions

Two different forcing frequencies corresponding to a Strouhal number of 0.02 ($f=900$ Hz), and 0.13 ($f=5$ kHz) and an unforced baseline were extensively studied; as noted above, both were JRG modes. Three other excitation frequencies ($f=1.8$, 2.67, and 10 kHz) were also tested but the impact of the excitation frequency on mixing and penetration was most receptive to 5 kHz excitation. Side- and end-view images were acquired for these three cases at one momentum flux ratio, r, of 1.7. x, y, z in each of the images correspond to the streamwise, transverse, and spanwise directions, respectively, and $x=0$, $y=-0.11D_e$, and $z=0$ corresponds to the center of the jet exit. The per-pixel spatial resolution, both for the side- and end-view images, was about 0.26 mm. An estimate of large-scale structure length scale based on $\mathrm{St}_D = 0.3$ was computed and found to be 13 mm. It should be mentioned that the camera resolution was not fine enough to resolve the Batchelor length scale. At least 200 images were acquired at each condition. Each image was *processed* by subtracting a background image and dividing by a normalization (flat field) image that accounts for variations in the laser intensity profile and other image nonuniformities (e.g., camera fixed pattern noise). Both the side- and end-view flat field images were obtained by averaging 100 instantaneous images without injection. The end-view images have been stretched in the spanwise direction to preserve the aspect ratio of the pixel array, which was necessary due to the oblique camera orientation and the resulting perspective distortion. Analysis was performed on these corrected instantaneous and time-averaged end- (spanwise-) and side- (streamwise-) view images. The images are presented in gray scale with black representing the lowest signal intensity corresponding to pure jet fluid and highest signal intensity, white indicates pure free stream fluid. The images are not time correlated

III. RESULTS AND DISCUSSION

A. Side-view images

Side-view images at the spanwise centerline of the injector ($z/D_e=0$) were acquired for the two forced cases (St $=0.02$ and 0.13) and the unforced baseline. The flow direction is from left to right. The injector was mounted on the top wall, and hence the images are presented in the same orientation. Each side-view image spans 5.5 jet diameters both in the streamwise and transverse directions. Temporally uncorrelated images were collected at two adjacent streamwise locations. The intensities, I, were rescaled using

$$I_{\mathrm{norm}i,j} = \frac{I_{i,j}}{I_{\max}}, \tag{1}$$

where

$$I_{\max} = \max(I_{i,j}). \tag{2}$$

Such that low values of I_{norm} closer to 0 (black) corresponds jet fluid and lighter regions corresponds to $I_{\mathrm{norm}} > 0$ represent both mixed and free stream fluids.

Figures 4–6 show two sample instantaneous side-view images for the three cases studied: baseline, St=0.13, and 0.02, respectively. In these images $y=0$ corresponds to a displacement of $0.11D_e$ from the injection wall. Regions closer to the wall were not imaged due to presence of strong scattering from the tunnel floor. Some of the salient features in all these images are the presence of large scale structures on the jet windward side, the three-dimensional bow shock, and

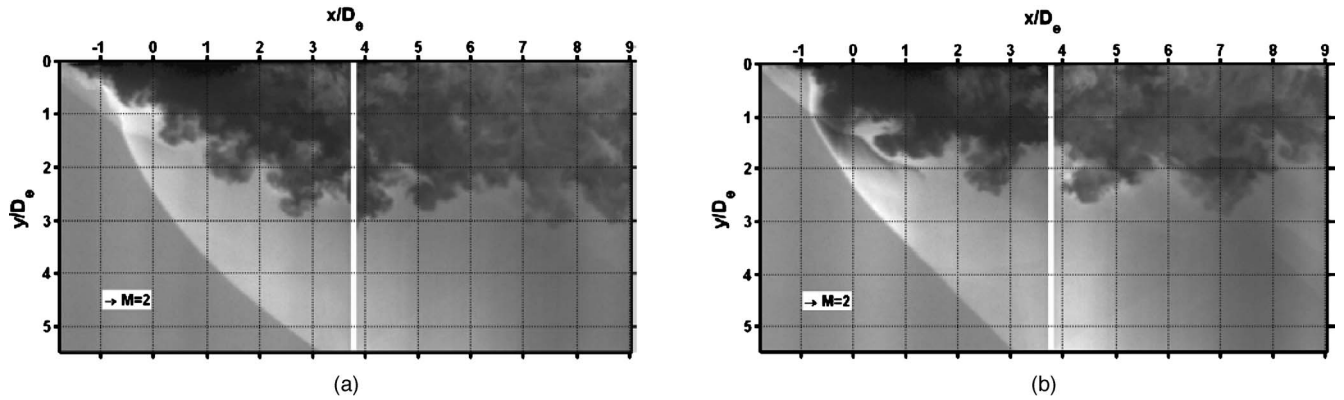

FIG. 5. Side-view images of instantaneous jet/free stream mixing: 5 kHz (St=0.13) forcing frequency. (a) and (b) are independent sample images composed from two independent measurements (and locations).

the separation shock upstream on jet windward side. The jet core is found to be relatively coherent at the first streamwise location, but it begins to breakdown and become amorphous as the injectant convects downstream. As the jet bends toward the cross stream, the signal intensities were found to increase indicating mixing between the jet and free stream. These features are more apparent when we compare the two images at the two streamwise locations adjacent to each other. The strong interaction of the large-scale structures with the separation shock creating a compression region (denoted by a lower normalized intensity) is also apparent in some of the images (right-hand side image in Fig. 5 and left-hand side image in Fig. 6). The dynamic nature of the flow is clearly visible when we compare instantaneous images. Some of the differences in these images are highlighted. In the baseline images, the bow shock is situated closer to the injection wall on the right image, whereas on the left image the shock is displaced above the injection wall due to the penetration of the jet into the upstream boundary layer. Between $4<x/D_e<9$ the free stream seems to have penetrated the jet core in the left-hand side image, and hence the intensity levels shift more toward the higher end (lighter color); in the right-hand side image, however, the core is still coherent until eight jet diameters. The local curvature of the bow shock is also found to vary due to the presence of the large-scale jet vortices. In the right image of Fig. 5, the jet eddy pushes the bow shock upstream near the injection wall. Similar features where the jet structure affects the local curvature of the bow shock have also been observed by Gruber *et al.*[26]

There is marked variation between the forced cases and the baseline case in the size and shape of large-scale structures on the windward side. The baseline cases have vortices which are much smaller in size when compared to either of the forced cases. Distinct vortex structures are seen on the windward side extending to the farthest streamwise measurement point ($=9.2D_e$) for the forced cases in the sample images. This arises due to the effect of forcing in the jet stream. Two-component-laser doppler velocimetry measurement of the HFA in a quiescent stream indicates that the axial velocity fluctuates up to 28% of the mean near the jet exit.[18] In the forced cases this causes modulation of the jet stream that leads to the formation of these distinct large-scale structures observed in the jet shear layer. These large-scale structures strain the interface between the jet and the free stream providing more interfacial contact. This would enable better mixing between the two streams. Lee *et al.*[1] identified jet-shear layer to be a primary location where combustion took place. Increasing the interracial contact would of course be beneficial for burning, since it provides greater potential flame surface (or at least a larger region of flammability).

Figure 7 shows the trajectory of the upper boundary of

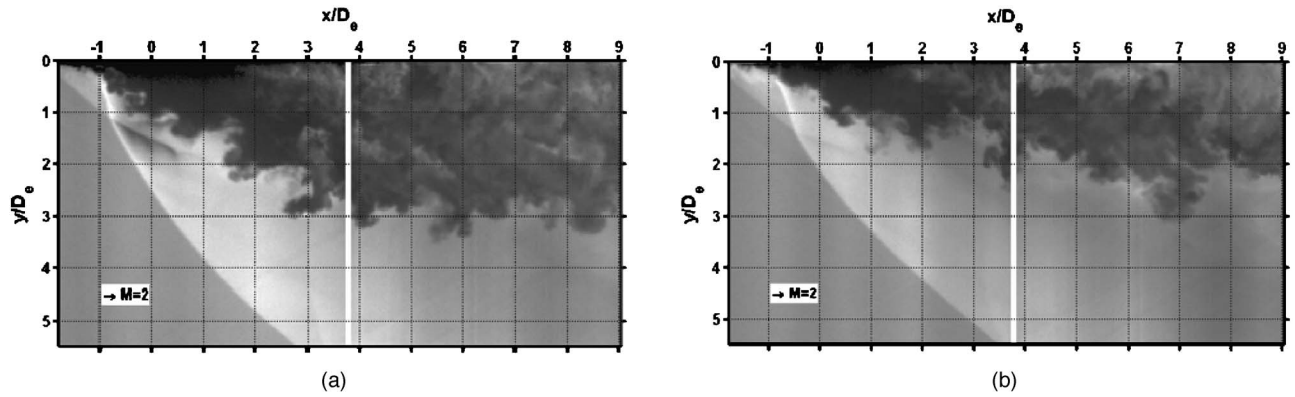

FIG. 6. Side-view images of instantaneous jet/free stream mixing: 900 Hz (St=0.02) forcing frequency. (a) and (b) are independent sample images composed from two independent measurements (and locations).

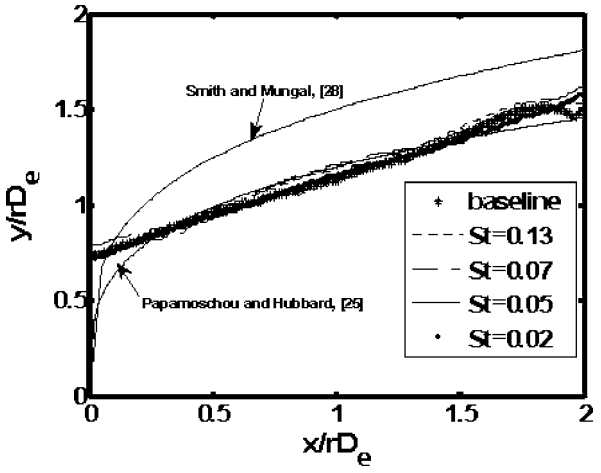

FIG. 7. Average transverse penetration of the jet for the forced and baseline cases (boundary marked at 90% of free stream intensity).

the jet for all the cases from Rayleigh/Mie scattering. The upper boundary of the jet was identified from the time-averaged images as the location that corresponds to 10% of the free stream intensity. The plot was scaled by the product r and D_e. r is the effective velocity ratio defined as $(\rho_j U_j^2/\rho_{\mathrm{cf}} U_{\mathrm{cf}}^2)^{1/2}$, where ρ is the density and U is the velocity, and the subscripts j and cf correspond to jet and cross flow, respectively.

The rD_e length scale was used by Pratte and Baines[27] to collapse the centerline jet trajectories at different r using the correlation given in Eq. (1)

$$x/(rD_e) = A(y/rD_e)^m. \tag{3}$$

The constant A and the exponent m have been used by several other researchers to scale their data.[1–3,24,25,27,28] Though the data showed a power-law trend, both A and m were found to vary between experiments. The rD_e-scaled trajectories collapse the data for the different cases fairly well. Circular jet trajectories from incompressible[28] and compressible[25] cases have also been added to the figure. The forced and baseline cases show similar average penetration to that of a compressible circular jet in supersonic cross stream. Since the flow is highly dynamic, as seen from the instantaneous images, the penetration of the jet in the forced cases would be governed by the large-scale structures in the jet shear layer; hence, the standard deviation images discussed in the following section would provide a better marker of the free stream and jet interface.

B. Side-view standard deviation

Standard deviation images for the baseline and two forced cases (St=0.13 and 0.02) are shown in Figs. 8(a)–8(c). These images were rescaled and normalized using

$$\sigma_{\mathrm{norm}i,j} = \frac{\sigma_{i,j}}{\sigma_{\max}}, \tag{4}$$

where

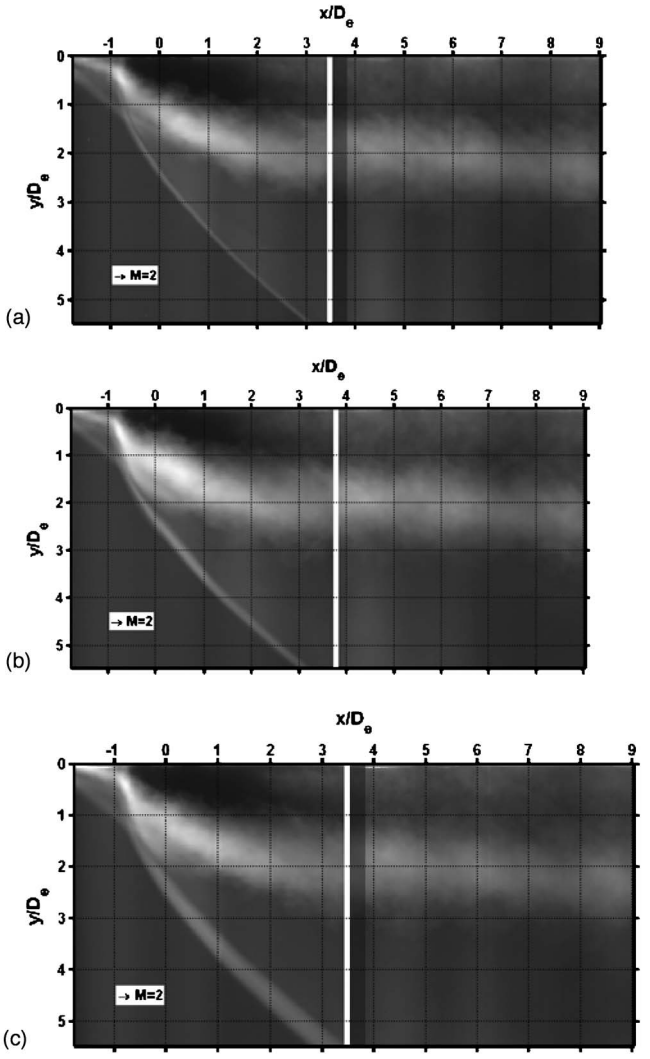

FIG. 8. Side-view images of the mixing standard deviation: (a) baseline, (b) St=0.13, and (c) St=0.02. Again, the images are composites from two probe locations.

$$\sigma_{\max} = \max(\sigma_{i,j}). \tag{5}$$

$\sigma_{\mathrm{norm}}=0$ would correspond to nonfluctuating free stream and jet cores and values of σ_{norm} approaching 1 would correspond to the regions of high fluctuation such as the shear layer.

The bow shock fluctuates slightly in the baseline case as indicated by the light arcing above the jet; the two forced cases, however, show a broader region of high standard deviation due to stronger fluctuations in the bow shock position. An earlier study by Gruber *et al.*[26] indicates that the unsteadiness of the bow shock near the jet exit arises from the intermittent nature of the large scale eddies formed on the windward jet side. In the present study, the higher fluctuation region around the bow shock in the forced cases arises due to varying jet momentum. The jet momentum varies over time as governed by the excitation frequency. At certain time instances the velocity of jet would fall below the mean value, hence the momentum of the jet would be lower and so the shock would be able to push itself downstream; at other instances the momentum of the jet is higher than the mean, and

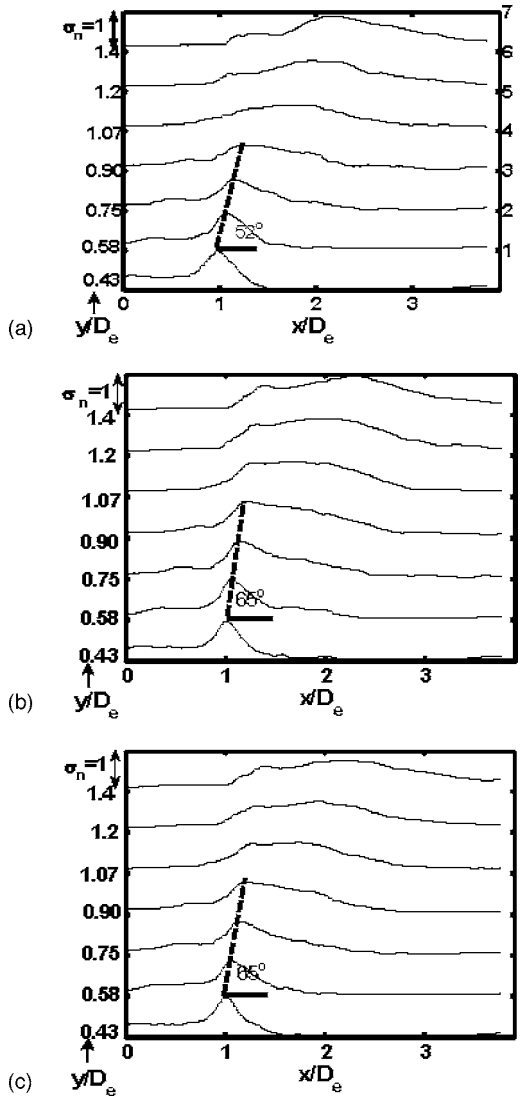

FIG. 9. Side-view standard deviation horizontal line plots at seven transverse locations from $y/D_e=0.43$ to 1.4 (a) baseline, (b) St=0.13, and (c) St=0.02.

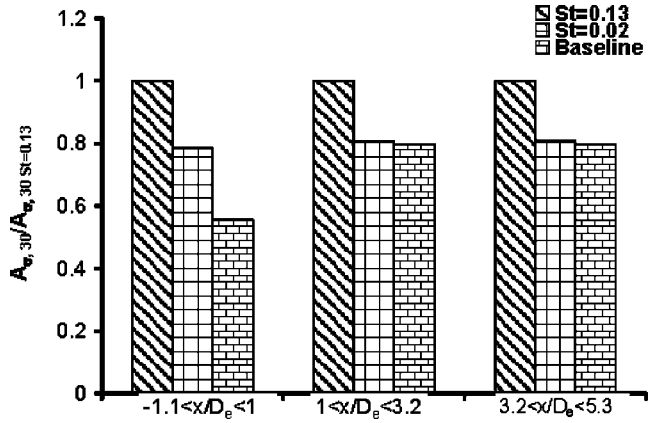

FIG. 10. Normalized mixing region area ratio ($A_{\sigma,30}\geqslant 0.3$) with a value of 1 corresponding to St=0.13 case from side-view standard-deviation images.

hence the jet structure would be able to push the shock upstream. All the three cases showed clearly the separation shock upstream of the injector exit as a smeared region with low fluctuations indicating unsteady nature of the lambda shock. High fluctuations were observed for the forced cases in the region where $0<y/D_e<2$ and $-1<x/D_e<0$. This occurs due to the formation of the periodic large-scale eddies which penetrate deep into the free stream entraining the cross stream fluid. Figures 9(a)–9(c) shows series of streamwise line plots obtained from the standard deviation images at nine transverse locations for the three cases. Overlaid on these plots is a line connecting the maxima for each line plot at the first four transverse locations. Distinct maxima are observed in the first four transverse locations. This feature corresponds $(x<1D_e)$ to the bow shock. There is a second maxima which is apparent at $y/D_e=1.2$ and 1.4 that indicates the jet and free stream interface. The line plots also show the development of the interface for all the cases. The jet-free stream interface is closer to the bow shock near the nozzle exit, and hence it appears as a single peak. The jet-free stream interface eventually becomes a broad band of mixed fluid as the jet is turned by the free stream. The slope of the free stream interface is also shown in the figure. Both the forced case have the same slope ($\theta=65$), which is 25% higher than the baseline. The reason for this higher slope could be due to the effect of pulsations that allow the large-scale structures penetrate deeper into the cross stream for the forced cases. Since the momentum of the jet varies with time, an impulse force is created during part of the cycle where the momentum increases from a low value to the maximum value over a finite time. Hence the jet inertial force is able to push the eddies deeper into the free stream enhancing the entrainment during this time interval. During the other part of the cycle, the free stream is able to penetrate deep into the jet due to the minimal hindrance from the jet. This enables effective large-scale mixing of the jet and free stream. Randolph *et al.*[17] also suggest that there is a finite time interval before the Mach disk is established in the flow. During this period the pulsating injectant is able to penetrate into the flow with little hindrance from the shock effect. On the other hand, the Mach disk, an established phenomenon in underexpanded jets in cross flow, limits the penetration depth of the jet.

To quantify the region involved in large-scale mixing for the three cases, an arbitrary value $\sigma_{\text{norm}}=0.3$ was chosen. The area enclosed within the jet boundary which had a $\sigma_{\text{norm}}\geqslant 0.3$ was computed. These mixing areas were normalized by the corresponding area value at St=0.13 for three region and presented in Fig. 10. This normalization would set the value for St=0.13–1 in all the three regions, emphasizing the change in mixing area relative to the forced St =0.13 case. At all the three regions, the St=0.13 case shows larger regions involved in large-scale mixing than the baseline and St=0.02 cases. This does not quantify small-scale or molecular mixing, since the Batchelor scales were smaller than the image resolution; rather, the area enclosed by $\sigma_{\text{norm}}\geqslant 0.3$, $A_{\sigma,30}$, can be thought of as the mixing potential since it could contain both small scale and bulk mixing. Relative to the baseline, $A_{\sigma,30}$, with St=0.13 is 25% greater in the region $1<x/D_e<5.3$ and 45% greater in the region

$-1<x/D_e<1$. For the St=0.02 in the region $-1<x/D_e<1$, $A_{\sigma,30}$ was found to be 23% greater than the value in the unforced baseline case. This large improvement in the forced cases clearly arises due to the formation of larger turbulent eddies that enhance mixing on the jet windward side near the jet exit. At greater streamwise distances, the $A_{\sigma,30}$ for the baseline and St=0.02 cases are nearly identical at about 80% of the area of the St=0.13 case.

C. Probability density functions

The instantaneous images show the dynamic nature of the flow field, which is crucial in understanding the mixing processes for different cases.[1–4] The presence of large- and small-scale structures, which play an active role in flow interaction, development and growth of the jet in cross stream, cannot be observed in the time-averaged field. Probability density functions (PDFs), have been used as a tool to identify the transport characteristics of mixing layers. A passive scalar probability density function measures the probability of occurrence of all mixture fractions at various locations within the mixing layer. One key concern in measuring the PDF of a mixing flow is its probe resolution. The resolution of the probe should be finer than the diffusion scales to prevent ambiguity in measuring the correct mixture fraction, since any signal indicative of a well mixed fluid could results from an average of unmixed fluid when the resolution is coarse. Such disparities between probe resolution and the flow scales are beyond the capabilities of even optical diagnostic techniques at high Reynolds number.[29]

The PDFs of signal intensities were calculated at various locations in the flow field for the side-view images from Mie scattering. These PDFs show the probability of occurrence of a specific signal intensity at a flow-field location. Normalized signal intensities (I_{norm}) with values close to 1 (white) correspond to free stream fluid and 0 (black) correspond to pure jet fluid. A value between 0 and 1 corresponds to mixed fluid. PDFs provide an indication of the mixture fraction at various locations on a pixel-sized basis. Though this cannot be used to quantify mixing at a molecular scale, it could be at least used to characterize the probability of large-scale mixing on a pixel basis.

The individual PDFs were constructed from the discrete intensity histograms at each location. 1000 samples (including four neighboring points) from the 200 instantaneous images at each location along the jet penetration trajectory (see Fig. 7) were used to construct the PDFs. The PDFs was then scaled by the bin width ($\Delta I/I_c$) The intensity values were normalized at each streamwise location by the maximum intensity (I_c). Probabilities of 1 and 0 would correspond to pure jet fluid and free stream fluid, respectively. The integration of the area under the PDF at every location equals unity by definition.

Figures 11(a)–11(c) show PDFs for the baseline and St=0.13 cases at three axial locations (x/D_e=0, 1 and 2) at the jet upper boundary in the flow field. At all the locations for the high-frequency forcing (St=0.13), the PDFs are broad, which indicates a wider variation of jet, free stream and mixed fluid consistent with the presence of large-scale eddies

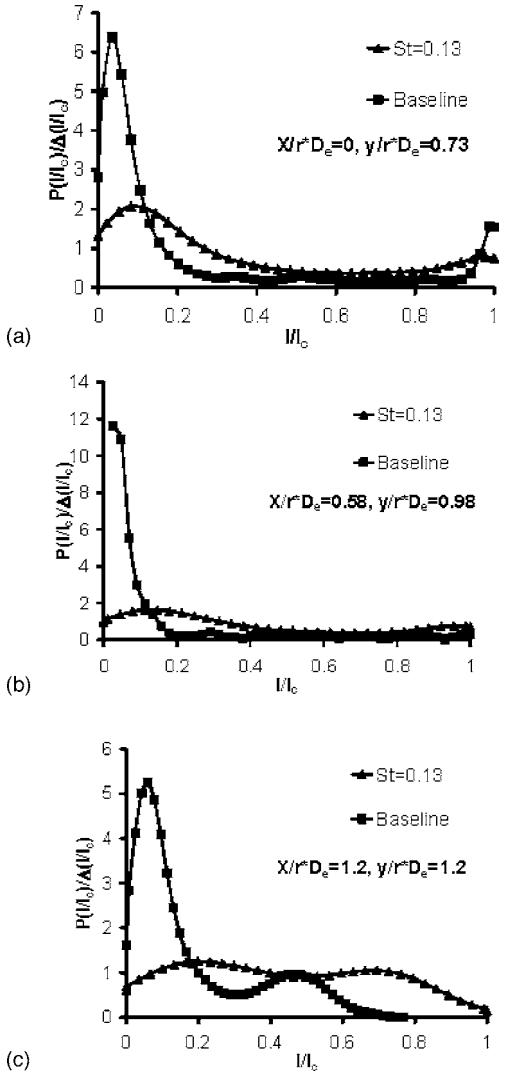

FIG. 11. Side-view PDF plots at jet upper trajectory, x/D_e= (a) 0, (b) 1, and (c) 2.

observed in the instantaneous images in the forced cases. It could also be observed that the baseline shows a high probability of finding jet fluid at all the three x location which indicates the jet core is more coherent whereas the forced case could indicate an amorphous nature of the jet due to the wide variation in the normalized intensities.

D. End-view images

The cross-sectional or end views were acquired for all the three cases at three different streamwise locations. x/D_e =−0.36, 2.1, and 8.3. Figures 12(a)–12(g) show selected instantaneous images for St=0.13 case at these three locations. Two sample images are presented at x/D_e=−0.36 and 8.3 and three snapshots at x/D_e=2.1. Each end-view image covers about 5.4 jet diameters in the spanwise (z) direction and 4.5 diameters in the transverse (y) direction. The images were normalized in the same way as in the side-view images [see Eqs. (1) and (2)].

All images show the development and the unsteadiness of the bow shock. Also prominent in these images are the presence of large-scale structures that form at the interface of

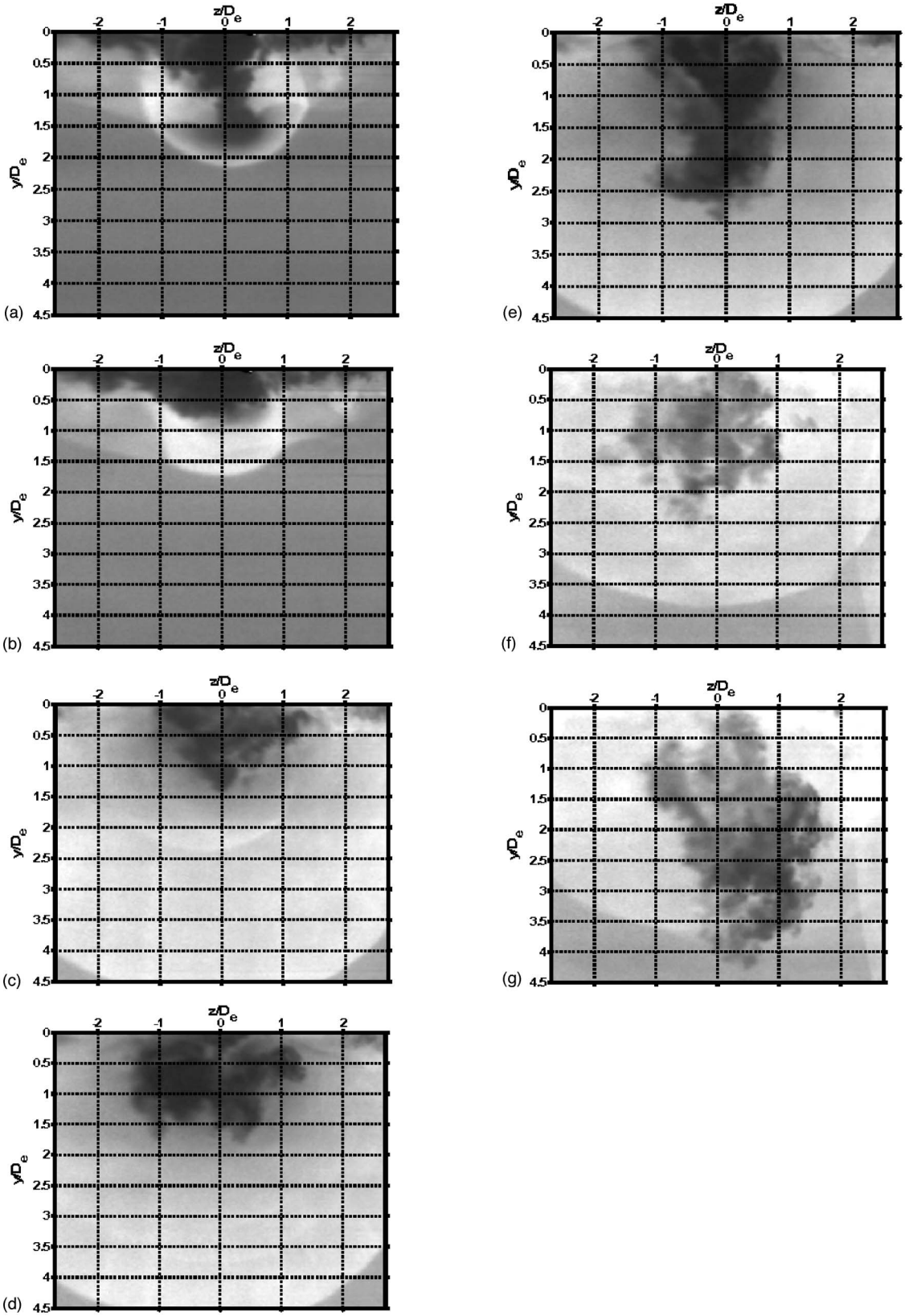

FIG. 12. (a)–(g): End-view images of the instantaneous jet/free stream mixing: 5 kHz (St=0.13) forcing frequency at different streamwise positions (x/D_e =−0.36, 2.1, and 8.3).

the jet and free stream. Figures 12(a) and 12(b) also show the penetration of the jet fluid in the boundary layer. There is also a marked difference in Figs. 12(a) and 12(b) taken at the same location at different time instances in terms of penetration. In Fig. 12(a) the jet structure penetrates deep into the crossflow, pushing the separation shock and creating a compressing region; in Fig. 12(b), however, the jet is devoid of any large eddies and penetrates 50% less than the jet shown

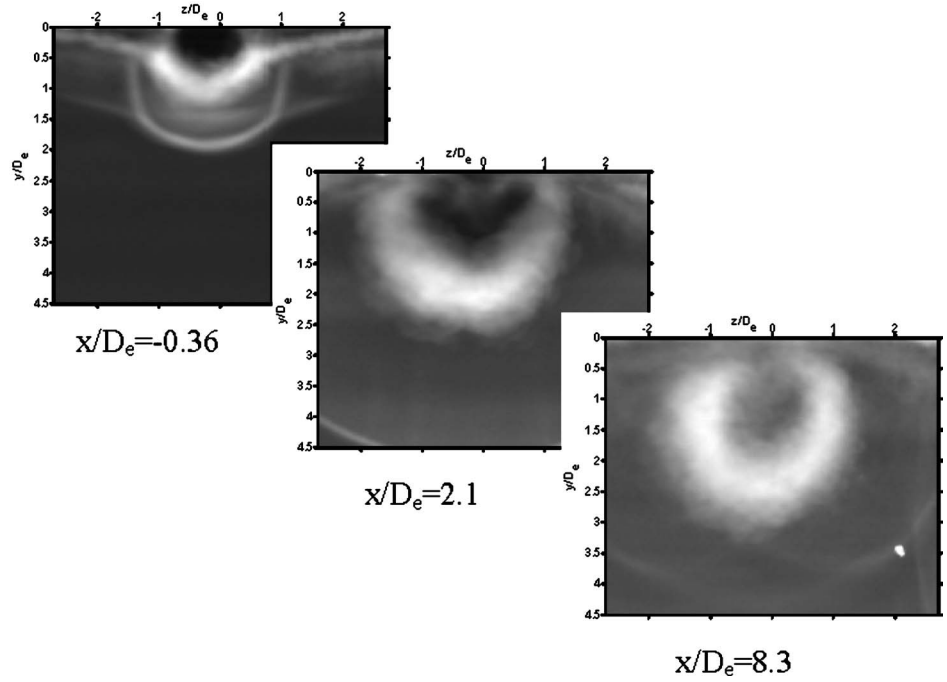

FIG. 13. End-view images of the mixing standard deviation: no forcing (baseline) at different streamwise locations (x/D_e=−0.36, 2.1, and 8.3).

in Fig. 12(a). Figures 12(c)–12(e) were all taken at x/D_e =2.1. There is a significant variation in the jet structures and the penetration depth. The jet structures appear to be breaking down in Fig. 12(c), enhancing mixing between the two streams. Figure 12(d) shows the presence of two separate asymmetric lobes on either side of the center line, and this resembles the counter-rotating vortex pair observed in other studies of compressible transverse jets.[2–4] This vortex pair advects unmixed cross-flow fluid into the bottom of the jet plume. Figure 12(e) shows high penetration with the jet core being amorphous with minimal intrusion from the free stream. The three snapshots at x/D_e=2.1 emphasize the dynamic three-dimensional turbulent nature of the flow. Figures 12(f) and 12(g) correspond to the single-shot images at x/D_e=8.3. Both images show highly disorganized structures with intensity values consistent with the significant jet-free stream mixing, unlike images at x/D_e=−0.36 and 2.1.

E. End-view standard deviation images

Figures 13 and 14 show the end-view standard deviation images for the baseline and St=0.13 cases at three streamwise locations. A similar normalization was adopted as in side-view standard deviation images [see Eqs. (4) and (5)]. The bow shock is visible as a thin arc in all the images. Both x/D_e=−0.36 and 2.1 show the presence of an undisrupted jet core. The St=0.13 case at the first location also shows high fluctuation until the bow shock; this arises due to the penetration and mixing of jet-shear layer vortices (see Figs. 5 and 6). At x/D_e=2.1 a crescent-like shape is observed for both cases indicating the counter rotating vortex pair observed in the plume. The jet looks elongated with high fluctuation existing until three jet diameters in the forced case. Further downstream the jet core starts to disappear due to the amorphous nature of jet observed in the instantaneous images. The forced case (St=0.13) also shows a wider band of fluctuation on the jet periphery when compared to the baseline.

To quantify the effects of mixing, three different parameters were studied. The first parameter was obtained from the time-averaged images. An area enclosed by the 90% intensity contour, A_{90}, was computed. This provides an indication of the area enclosed by the jet fluid and the entrained free stream fluid. The second parameter, the mixing region area, $A_{\sigma,30}$, was obtained from the standard deviation images. As before, this refers to the area associated with standard deviation of $\geqslant$30%. The third parameter, the shape parameter S, was computed from the perimeter P of the mixing area:

$$S = \frac{P}{2\pi r_o},$$

where

$$r_o = \sqrt{\frac{A_{\sigma,30}}{\pi}}. \tag{6}$$

All three parameters have been used in jet injection studies. Grube *et al.*[3] used them for a transverse jet in a supersonic cross flow and Glawe *et al.*[30] for a parallel injection into a supersonic stream. The shape parameter shows the degree of mixing potential afforded by the injection scheme and defines the relationship between the perimeter and the area of a given contour compared to a perfect circle. A shape parameter of 1 would indicate a circle and low mixing potential; values of $S>1$ would indicate higher interfacial contact due to large straining of the jet-free stream interface and thus a higher degree of mixing.

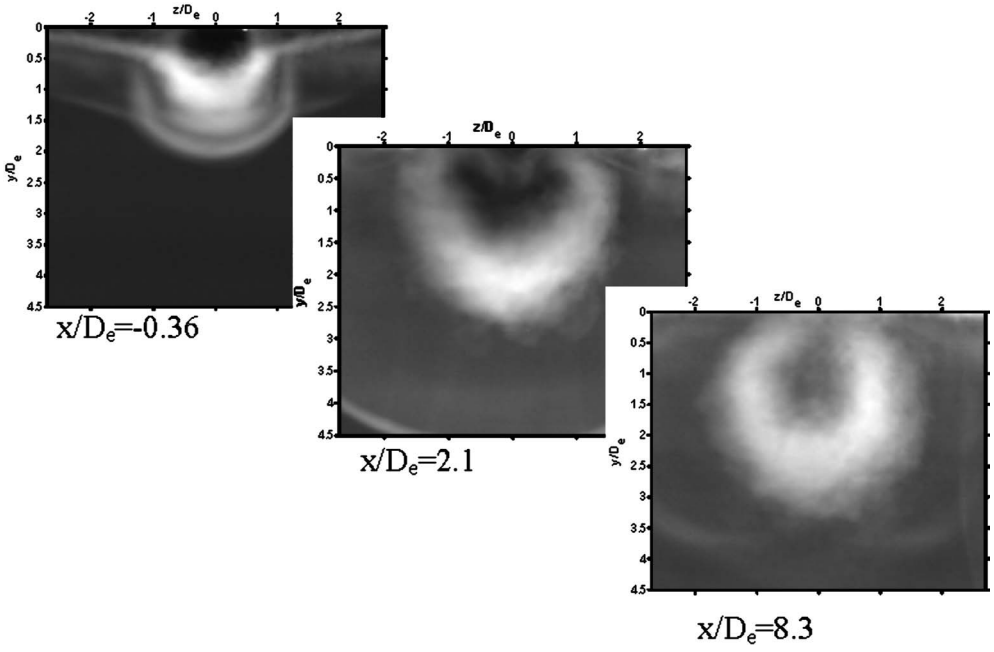

FIG. 14. End-view images of the mixing standard deviation: 5 kHz (St=0.13) forcing frequency at different streamwise locations (x/D_e=−0.36, 2.1, and 8.3).

Figures 15, 16, and 17 show the respective values of A_{90}, $A_{\sigma,30}$, and S, for the two forced cases (St=0.13 and 0.02), and the baseline case. Error bars are indicated assuming ±10 pixel uncertainty in determining the jet boundary. In order to emphasize the variation of these parameters, each has been normalized by the corresponding value from the baseline case.

The normalized mean plume area ($A_{90}/A_{90,\text{baseline}}$) from Fig. 15 initially increases and then decreases for the forced cases; nonetheless, the mean area was found to be higher for the first four jet diameters. Past four jet diameters, A_{90} was found to be comparable to the baseline values and even lower at 8.3 jet diameters for the St=0.02 case. This could indicate higher entrainment of the free stream into the jet boundary in the first four diameters for the forced cases. The peak A_{90} was found to be 36% higher than baseline for the high frequency case, whereas at St=0.02 the maximum was 42% higher than baseline. The mixing area ratio is shown in Fig. 16. There was no consistent trend with respect to x/D_e observed between the forcing cases, but it was found that the forced cases had higher mixing area when compared to the baseline for almost all the location studied. The increase in the maximum mixing area for both the forced cases was found be less than 15%. The shape parameter S is shown in Fig. 17. The secondary y axis on the right shows unnormalized values of the shape parameter for the baseline. The values are found to be much higher than 1 in the near field, indicating a strained interface, which is beneficial for mixing, but further downstream the S parameter approaches 1, indicating that the contours tend to become more circular. As with the other two parameters, the forced cases show benefits over the baseline case due larger strained region that occur because of the presence of large-scale structures.

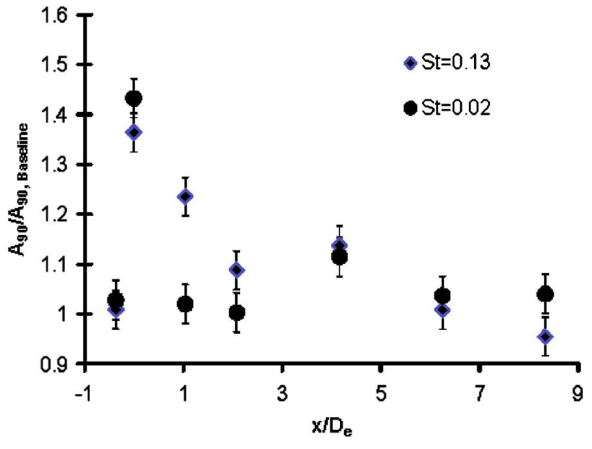

FIG. 15. Plume area ratio normalized by the baseline which represents the area enclosed by the jet fluid.

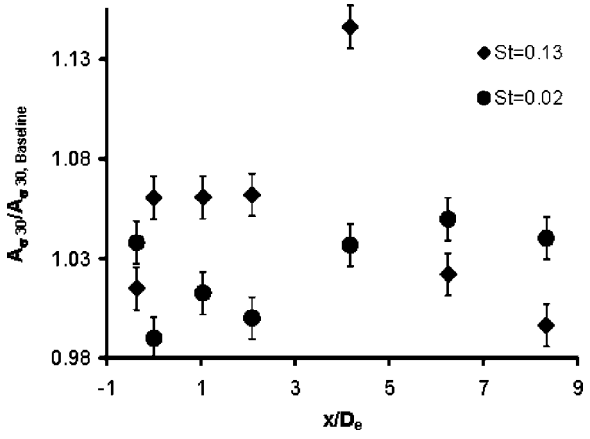

FIG. 16. Mixing region area ratio (area with standard deviation >0.3) normalized by the baseline representing the area involved in mixing within the jet fluid boundary.

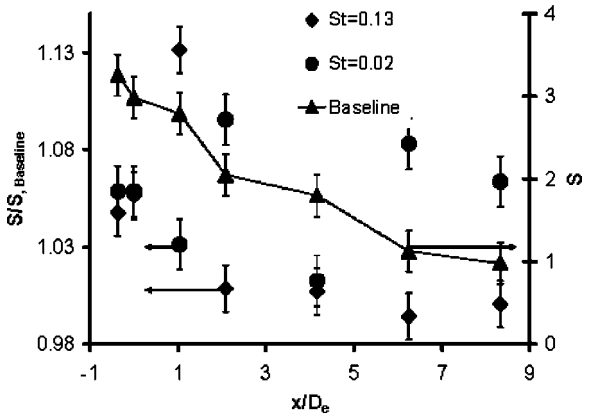

FIG. 17. Mixing region shape factor, *S*, normalized by the baseline value, representing the interfacial contact between the jet and free stream. The right-hand axis shows the shape factor magnitude (not normalized) for the baseline case.

Based on the results from the three parameters, the forced cases indicate better entrainment and mixing characteristics in the entire measurement region.

IV. CONCLUSIONS

Transverse injection of a novel high frequency actuator (HFA) in a Mach-2 cold cross flow was studied. The primary method employed was laser scattering from small, naturally occurring flow-field ice particles that mark the free stream. Three jets conditions corresponding to Strouhal numbers (St, based on jet diameter) of 0 (no excitation), 0.02 (excitation at 900 Hz), and 0.13 (excitation at 5 kHz) were selected for detailed investigation. Side- and end-view instantaneous scattering images show clearly the jet-fluid and free stream interface and indicate a highly three dimensional flow with rich vortical structures. Scattering images of the forced cases indicate large-scale eddies that appear periodically on the jet-free stream interface. These structures penetrate deeper into the free stream, in comparison to baseline jet large scale structures. The standard deviation images also indicate larger regions with bulk and small scale mixing with the forced cases, as compared to the baseline case; this primarily arises due to the higher interfacial contact area provided by the formation of the large-scale structures. Analysis from the end-view images also indicates higher entrainment and better mixing characteristics for the forced jets. For the current study both the forced cases (St=0.13 and 0.02) were found to provide superior mixing characteristics over the entire measurement range and higher penetration of the large scale structures into the free stream as compared to the baseline.

The current study indicates that forcing could be beneficial in mixing and penetration in supersonic flow. It should also be pointed out that forcing at a higher frequency $[O\ (1\ \text{kHz})]$ could lead to a much faster jet break up whereas low-frequency forcing produces turbulent puffs at regular interval which do not interact with each other.

ACKNOWLEDGMENTS

The financial support of the DAGSI Program along with AFOSR is gratefully appreciated. The authors would like to acknowledge Dr. Mark Hsu, Dave Schommer, and Bill Terry, Innovative Scientific Solutions, Inc., for their help and support in setting up the experiments.

[1] M. P. Lee, B. K. McMillin, J. L. Palmer, and R. K. Hanson, "Planar fluorescence imaging of a transverse jet in a supersonic cross flow," J. Propul. Power **8**, 729 (1992).
[2] J. C. Hermanson and M. Winter, "Mie scattering imaging of transverse, sonic jet in supersonic flow," AIAA J. **31**, 129 (1993).
[3] M. R. Gruber, A. S. Nejad, T. H. Chen, and J. C. Dutton, "Transverse injection from circular and elliptic nozzles into a supersonic cross flow," J. Propul. Power **16**, 449 (2000).
[4] W. M. VanLerberghe, J. G. Santiago, J. C. Dutton, and R. P. Lucht, "Mixing of a sonic transverse jet injected into a supersonic flow," AIAA J. **38**, 470 (2000).
[5] G. B. Northam, I. Greenberg, and C. S. Byington, "Evaluation of parallel injector configurations for supersonic combustion," AIAA Paper 89–2525 (1989).
[6] E. J. Gutmark, K. C. Schadow, and K. H. Yu, "Mixing enhancement in supersonic free shear flows," Annu. Rev. Fluid Mech. **27**, 375 (1995).
[7] J. M. Seiner, S. M. Dash, and D. C. Kenzakowski, "Historical survey on enhanced mixing in scramjet engines," J. Propul. Power **17**, 1273 (2001).
[8] I. J. Kalkhoran and M. K. Smart, "Aspects of shock wave induced vortex breakdown," Prog. Aerosp. Sci. **36**, 63 (2000).
[9] S. Menon, "Shock wave induced mixing enhancement in scramjet combustors," AIAA Paper 89–0104 (1989).
[10] R. C. Rogers, D. P. Capriotti, and R. W. Guy, "Experimental supersonic combustion research at NASA Langley," AIAA Paper 98–2506 (1998).
[11] F. E. Marble, E. E. Zukoski, J. W. Jacobs, G. J. Hendrick, and I. A. Waitz, "Shock enhancement of and control of hypersonic mixing and combustion," AIAA Paper 90–1981 (1990).
[12] A. D. Cutler and S. E. Doerner, "Effects of swirl and skew upon supersonic wall jet in cross flow," J. Propul. Power **17**, 1327 (2001).
[13] S. Narayanan, P. Barooah, and J. M. Cohen, "Dynamics and control of an isolated jet in crossflow," AIAA J. **41**, 2316 (2003).
[14] A. Eroglu and E. Breidenthal, "Structure, penetration, and mixing of pulsed jet in crossflow," AIAA J. **39**, 417 (2001).
[15] J. C. Hermanson, A. Wahba, and H. Johari, "Duty-cycle effects on penetration of fully modulated, turbulent jets in crossflow," AIAA J. **36**, 1935 (1998).
[16] H. Johari, M. Pacheco-Tougas, and J. C. Hermanson, "Penetration and mixing of fully modulated turbulent jets in crossflow," AIAA J. **37**, 842 (1999).
[17] H. Randolph, L. Chew, and H. Johari, "Pulsed jets in crossflow," J. Propul. Power **10**, 746 (1994).
[18] S. Murugappan and E. J. Gutmark, "Flowfield and mixing control of an underexpanded jet," AIAA J. **42**, 1612 (2004).
[19] M. R. Gruber and A. S. Nejad, "New supersonic combustion research facility," J. Propul. Power **11**, 1080 (1995).
[20] J. Hartmann and B. Trolle, "A new acoustic generator. The air jet generator," J. Sci. Instrum. **4**, 101 (1927).
[21] J. Hartmann, "Construction, performance, and design of the acoustic air-jet generator," J. Sci. Instrum. **16**, 140 (1939).
[22] V. Sarohia and H. L. Back, "Experimental investigation of flow and heating in a resonance tube," J. Fluid Mech. **94**, 649 (1979).
[23] S. Murugappan and E. Gutmark, "Parametric study of Hartmann-Sprenger tube," Exp. Fluids **38**, 813 (2005).
[24] R. C. Orth, J. A. Schetz, and F. S. Billig, "The interaction and penetration of gaseous jets in supersonic flow," NASA CR -1386, July 1969.
[25] D. Papmoschou and D. G. Hubbard, "Visual observations of supersonic transverse jets," Exp. Fluids **14**, 468 (1993).
[26] M. R. Gruber, A. S. Nejad, T. H. Chen, and J. C. Dutton, "Bow shock/jet interaction in compressible transverse injection flow field," AIAA J. **34**, 2191 (1996).

[27]B. D. Pratte and W. D. Baines, "Profiles of round turbulent jet in cross flow," J. Hydronaut. Div. ASCE **92**, 53 (1967).
[28]S. H. Smith and M. G. Mungal, "Mixing, structure and scaling of the jet in crossflow," J. Fluid Mech. **357**, 83 (1998).
[29]N. L. Messersmith and J. C. Dutton, "Mie scattering measurements of probability density functions in compressible mixing layers," Exp. Fluids **21**, 291 (1996).
[30]D. D. Glawe, M. Samimy, A. S. Nejad, and T. H. Chen, "Effects of nozzle geometry on parallel injection from base of an extended strut into a supersonic flow," AIAA Paper 95–0522, January 1995.